Retrofitting of box section concrete beams to resist shear and torsion using Near-Surface-Mount (NSM) GFRP Stirrups

Moaz A. Nasser
Civil Engineering Department, High Institute for Engineering Technology, 21K Cairo-Belbies Rd., Al-Obour, Egypt
Eng.moaz@oi.edu.eg, http://orcid.org/0009-0002-3014-4278

Ahmed A. Mahmoud, Tarek S. Mustafa, Ahmed N. M. Khater
Benha University, Faculty of Engineering at Shoubra, Civil Engineering Department, 108 Shoubra Street, Shoubra 11691, Cairo, Egypt.
ahmed.ahmed@feng.bu.edu.eg, http://orcid.org/0000-0003-2306-5950
Tarek.mohamed@feng.bu.edu.eg, http://orcid.org/0000-0002-0015-9113
ahmed.khater@feng.bu.edu.eg, http://orcid.org/0000-0003-4528-8979

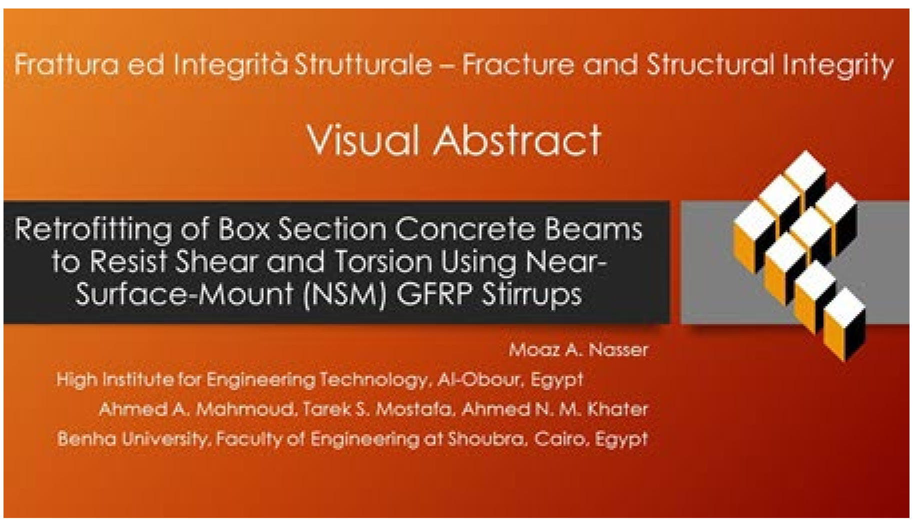

OPEN ACCESS

Citation: Nasser, M. A., Mahmoud, A.A., Mustafa, T. S., Khater, A.N.M., Retrofitting of box section concrete beams to resist shear and torsion using Near-Surface-Mount (NSM) GFRP Stirrups, Frattura ed Integrità Strutturale, 67 (2024) 319-336.

Received: 03.09.2023
Accepted: 09.12.2023
Online first: 14.12.2023
Published: 01.01.2024

KEYWORDS. Experimental, Analytical, Reinforced concrete box section beams, Near-surface mount (NSM), Retrofitting, Shear and torsion, glass-fiber-reinforced polymer (GFRP).

INTRODUCTION

There are three distinct subfields of research into torsion: combined shear and torsion, pure torsion, and combined torsion and bending. Studies including how supported cement footers behave in unadulterated twists began in 1929 when the first research determined torsional strength conditions in light of the 45° space truss model [1].

Glass fiber-reinforced polymer (GFRP) is a compound made of glass that is based on silica and can be made into different grades by adding metal oxides (Hearing [2]). Due to its chemical composition, it has excellent electrical insulation properties. Underlying, or S-glass, has higher strength and more noteworthy consumption opposition than electrical glass. Corrosion-resistant glass E-CR is one example of a hybrid that can be made [2].

Manufacturers of glass fibers have recently obtained increased strength and corrosion resistance in extreme chemical attack environments. With the growth of the polymer industry, fiber-reinforced composite structures have become an alternative to traditional building materials in many industries. Due to their superior mechanical strength, impact resistance, and corrosion resistance, fiber-reinforced polymer (FRP) composite materials are utilized in the aircraft, automobile, and ship industries. According to Chidananda and Khadiranaikar [3], GFRP bars, which are chemically inert and noncorrosive, can help significantly extend the lifecycle of reinforced concrete structures and reduce the costs of their maintenance, repair, and replacement.

A novel technique for reinforcement known as near-surface mounted (NSM) has emerged. This method entails creating a groove within the concrete cover and inserting bars into it, secured by a specialized filler like epoxy or cement mortar. This approach enhances its effectiveness and stands as a viable method. Moreover, compared to external bonding techniques, the NSM method offers a swifter, simpler, and more efficient application [4].

Certain scholars examined the application of FRP bars for enhancing the flexural reinforcement in concrete beams [5, 6]. Numerous investigations focused on fortifying reinforced concrete elements through the utilization of the NSM approach with materials such as CFRP bars [7-9], CFRP strips [10], GFRP laminates [11], CFRP laminates [12], CFRP rods [13-17], and AFRP rods [18].

The NSM FRP has become an attractive method for strengthening RC members and masonry, increasing their flexural and shear strength. In this technique, the FRP reinforcement is bonded into grooves cut into the concrete cover. The NSM FRP technique has been used in many applications, and it presents several advantages over the EB FRP technique in strengthening concrete structures and masonry walls.

The details of the procedure for the installation of NSM GFRP laminates and bars on concrete members can be found in [19-23]. Two methods are used to form the grooves. The application of NSM ropes in concrete using the first method is as follows:

1. Slits were cut in the concrete cover on the tension face of the beam using a diamond cutter.
2. The compressed air was used to clean the slits.
3. The GFRP ropes were cleaned with liquid acetone.
4. The epoxy adhesive was applied to the GFRP ropes.
5. The GFRP ropes were introduced into the slits, and the excess epoxy adhesive was removed.

The second method is an easy way to make grooves. Before concrete casting, plastic or wood strips with the dimensions of the needed grooves are installed over the wooden mold in the positions needed. After concrete curing, the plastic or wood strips were removed, and the grooves were left at the bottom or side surface of the beam.

The most important problem facing reinforced concrete structures is the corrosion of steel rebars. To struggle with the corrosion of rebars, it is better to use GFRP rebars instead of steel rebars. A few research studies are available on the behavior of reinforced concrete (RC) box section beams with fiber-reinforced polymer bars (GFRP) and GFRP stirrups under torsion. Consequently, the behavior of these beams needs to be investigated. In this study, the eccentricity of the applied load and the shear-span-to-depth (a/d) ratio were used to divide the tested specimens into three groups, as shown in Figs. 1 and 2. Each group had a single control specimen strengthened by NSM GFRP stirrups using various strengthening schemes (diameter, spacing, and inclination of external stirrups).

EXPERIMENTAL PROGRAM

The current investigation employed three factors to modify the tested specimens: (1) the diameter of external GFRP stirrups (Φ8, Φ10, and Φ12 mm), (2) the inclination of external GFRP stirrups (45º, 60º, and 90º), and (3) the spacing of external GFRP stirrups (75, 100, 125, and 150 mm). The dimensions of the specimens, their clear span, concrete grade, and internal GFRP longitudinal reinforcement remained consistent throughout the study. The experimental phase encompassed a series of tests conducted on standard concrete cubes, cylinders, and GFRP bars to determine their mechanical properties. The study involved monitoring, analyzing, and presenting aspects like initial crack loads, crack patterns, ultimate loads, failure modes, and strains in both concrete and external GFRP stirrups.

The experimental program consists of testing nine reinforced concrete box section specimens. One specimen was a control specimen; eight specimens were strengthened using NSM techniques with closed stirrups (external GFRP ropes). The chosen specimens were deliberately varied to encompass the entire spectrum of parameters under investigation. All specimens maintained a consistent size, featuring dimensions of 400 mm in width, 600 mm in overall depth, and 2200 mm in total length, with a clear span of 2000 mm. The shear span-to-total depth ratio (a/t) was set at three values: 0.67, 0.75, and 1.0. The experimental configuration involved subjecting the specimens to a four-point loading setup, as illustrated in Figs. 1 and 2. The pertinent details of the tested specimens are condensed in Tab. 1.

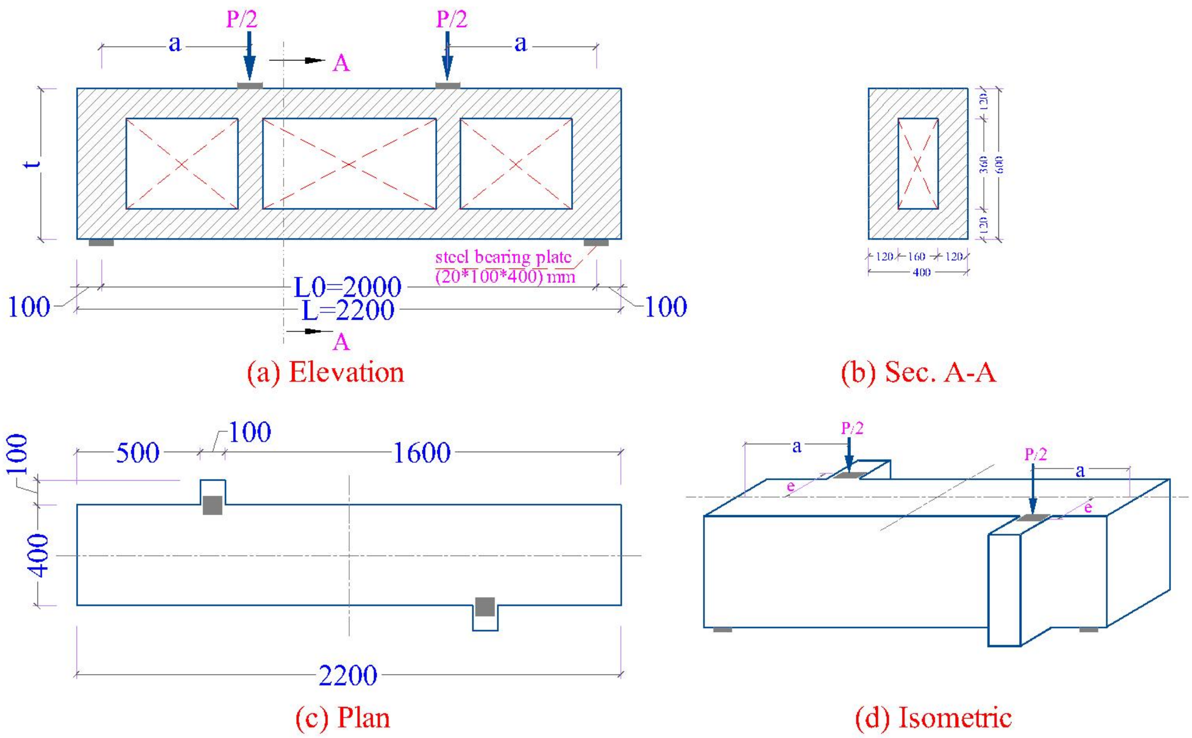

Figure 1: Specimen's details.

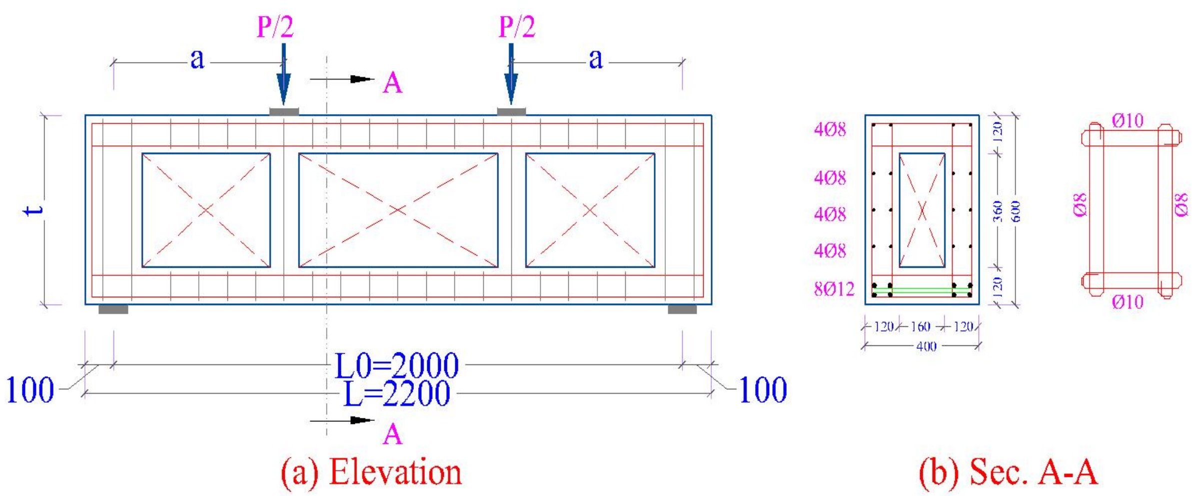

Figure 2: GFRP reinforcement details for the tested specimens.

The first group consisted of three specimens with a shear span of 600, 450, and 400 mm, corresponding to a shear span to total depth ratio (a/t) of 1.0, 0.75, and 0.67, respectively, with an eccentricity to specimen width ratio of (e/b`) 0.75. One of them is the control specimen (RB1), and the others are named RB2 and RB3. All of them were strengthened after testing by inclined stirrups at 45º with a diameter of Φ8, Φ 10, and Φ 12 mm bars spaced at 100 mm, as shown in Tab. 1.

The second group consists of three specimens with a shear-span-to-total depth ratio (a/t) equal to 1.00 with an eccentricity-to-specimen width ratio (e/b`) of 0.75. The strengthened specimens RB7, RB4, and RB5 had the same strengthening technique by stirrups with diameters Φ 10 spaced at 100 mm at an inclination 45º ,60º , and 90º, respectively.

In the third group, a 600-mm shear span was used, which equals a shear span to total depth ratio (a/t) of 1.00 and an eccentricity to specimen width ratio (e/b`) of 0.75. This group consists of four specimens: RB8, RB7, RB9, and RB6. The specimens in this group were strengthened by 45º inclined external stirrups spaced at 75, 100, 125, and 150 mm.

Before Strengthening									After strengthening			
Group No.	Specimen No.	a (mm)	(a/t) ratio	e (mm)	(e/b`) ratio (-)	Internal Vl. Web RFT (mm)	Internal Hz. Web RFT (mm)	Effect	External GFRP stirrups .	External stirrup inclination (degree)	External stirrup spacing	Effects of external stirrups
	RB1	600	1						10			
1	RB2	450	0.75	150	0.75	8	8	Shear-span to total depth	8	45	100	Diameter
	RB3	400	0.67						12			
	RB4			100	0.5					60		
2		600	1			8	8	Eccentricity	10		100	Inclination
	RB5			170	0.85					90		
	RB6					10	8	Vertical web reinforcement			150	
	RB7					12	8				100	
3		600	1	150	0.75				10	45		Spacing
	RB8					8	10	Horizontal web reinforcement			75	
	RB9					8	12				125	

Table 1: Details of the tested specimens (b`: Half the beam web width (200 mm); Vl.: Vertical web reinforcement; Hz.: Horizontal web reinforcement; and RFT: Reinforcement).

Mixture composition and material properties

Portland cement, CEM I 52.5 N, was used. Dolomite with a nominal size between 10 mm and 20 mm served as the coarse aggregate, and sand was used as the fine aggregate. For each specimen, the mix ratios of cement, fine aggregate, coarse aggregate were 1:1.95:3.65 by weight [24]. Water free from impurities was used for mixing and curing concrete. The used water-cement ratio is taken as constant for all mixes, equal to 0.47. The target grade of the concrete is 25 MPa. The properties of concrete in compression, tension, and elastic modulus are determined according to ASTM [25- 28]. Fig. 3 shows the stress-strain curve for concrete in compression.

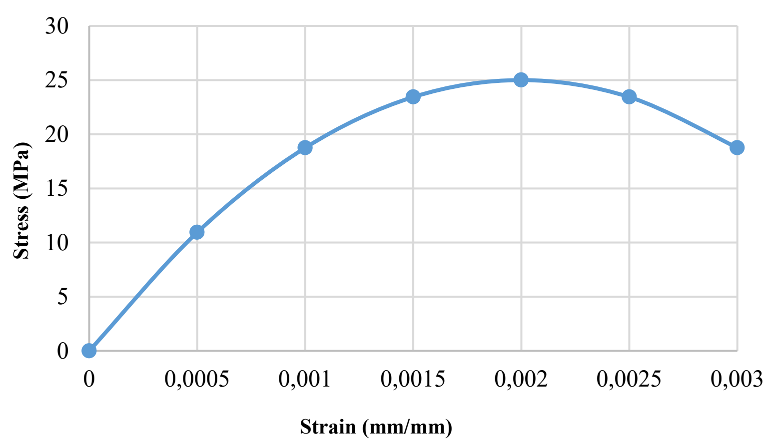

Figure 3: Stress-strain curve for concrete in compression.

Internal GFRP reinforcement bars and internal GFRP stirrups were made from ready-made GFRP bars. Tab. 2 shows the mechanical properties of the GFRP stirrups used in this study. Internal GFRP stirrups were fabricated using plastic elbows filled with epoxy to connect the GFRP bars at corners. Fig. 4 shows the testing of the internal GFRP stirrups.

Properties	GFRP bars		
Nominal diameter (mm)	8	10	12
Nominal area (mm^2)	50.29	78.57	113.14
Mass per meter run (gm/m)	90.3	138.0	205.0
Tensile strength (MPa)	1147.74	1027.36	1057.98
Elasticity modulus (GPa)	66	50	65

Table 2: Characteristic properties of the used ready-made GFRP reinforcement and internal GFRP stirrups from the manufacturing data sheet.

The external GFRP stirrups (ropes) are made from glass fiber ropes with the required diameter immersed in epoxy arsine and then applied to the strengthened specimens in the required positions. The mechanical properties of GFRP stirrups were obtained by testing samples of them. Fig. 5 shows the stress-strain curve for samples of the external GFRP stirrups according to ASTM [29].

Figure 4: Testing of the internal GFRP stirrup joint.

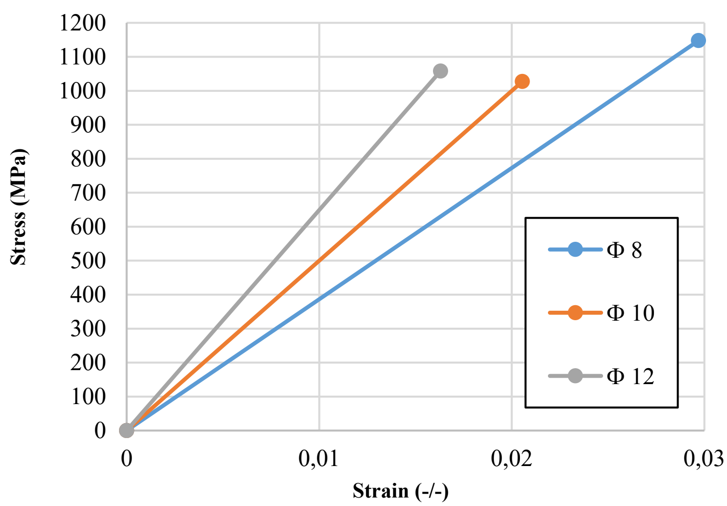

Figure 5: Stress-strain curves for samples of the external GFRP stirrups (ropes).

Properties	KEMAPOXY 150
Density	1.8–2.1 t/m^3
Compressive strength	50-100 MPa
Flexural strength	20-40 MPa
Tensile strength	15-25 MPa

Table 3: Mechanical properties of the used epoxy adhesive (from the manufacturing data sheet).

In this investigation, KEMAPOXY 150, an epoxy adhesive manufactured by the CMB company, was employed. This epoxy, designated for attaching NSM GFRP external stirrups to concrete, boasts numerous advantages. These encompass an extended pot life, a lengthy open time, solvent-free composition, a clear and colorless liquid epoxy resin with temperature resistance, easy mixing and application, high mechanical strength, remarkable resistance to creep under sustained loads, impressive durability against abrasion and impact, and swift curing even in low-temperature conditions. This epoxy comprises two components, denoted as (A) (white) and (B) (black), which are combined in a 2:1 ratio to yield the desired mixture (light grey). The blending process was conducted with an electric hand mixer for approximately 2 minutes, ensuring the elimination of color streaks within the mixture. The resin-hardener interaction initiates the pot life. The detailed technical specifications and mechanical properties of this epoxy adhesive are outlined in Tab. 3.

TEST SETUP, INSTRUMENTATION AND TEST PROCEDURE

The specimens underwent testing involving four-point bending until failure occurred. The experimentation took place within the laboratory facilities of the Engineering Faculty at the American University. The experimental configuration, as depicted in Fig. 6, involved securing the specimens within a sturdy reaction frame. The application of force was achieved through a hydraulic jack with a capacity of 2000 kN, linked to an electrical pump. Each specimen was affixed with a single linear variable displacement transducer (LVDT) at the midpoint to gauge deflection. To measure strain in the tension reinforcement, two strain gauges were affixed to the center of the lower GFRP bars, while another was attached to the stirrup. As the applied load progressively increased until reaching failure, the development of cracks was meticulously tracked. The collection of test data occurred via a data acquisition system that interfaced with a computer, and data was recorded at two-second intervals.

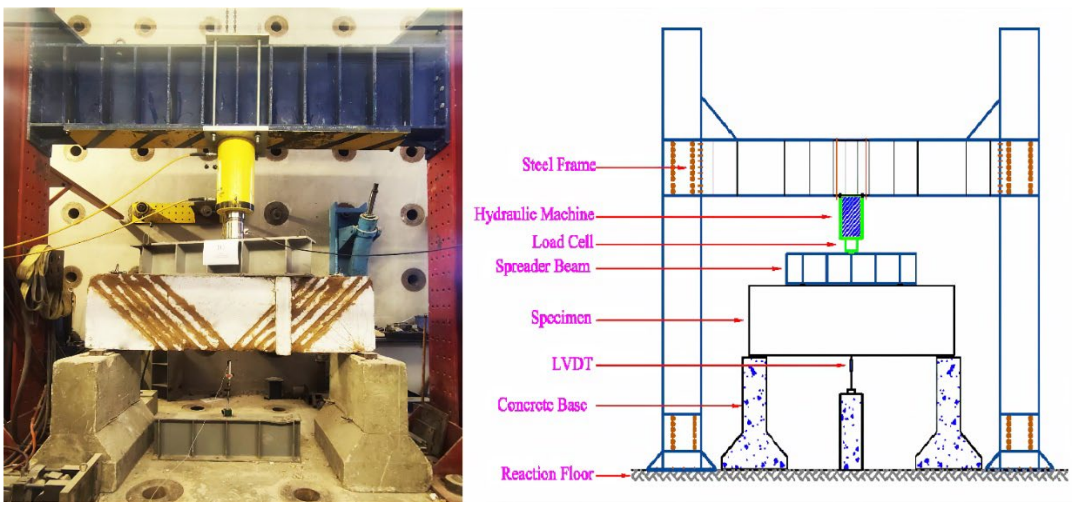

Figure 6: Test setup and instrumentations.

STRENGTHENING TECHNIQUE

The procedure for retrofitting the tested specimens using external GFRP stirrups can be summarized as follows:

1. The surface of the specimens was roughened by creating notches using an angle grinder;
2. Groves with diameters of 8, 10, and 12 mm + 2 mm were drilled at the arranged positions at spacing of 75, 100, 125, 150, and 200 mm with inclinations of 45, 60, and 90 degrees;
3. The surface of the specimens was cleaned with a wire brush and a blower with a high-pressure air jet;
4. A bonding agent was applied to the specimens' surface to enhance the connection between the original surface and the reinforcing NSM GFRP stirrups. The epoxy resin was then administered to the concrete surface in the region where the GFRP stirrups were positioned, utilizing a specialized tool.
5. External GFRF stirrups are immersed in the epoxy resin, then installed in their position; and
6. A mortar layer was applied and left for curing. Fig. 7 shows the tested specimens after retrofitting.

Figure 7: Tested specimens after retrofitting.

Analysis of the experimental results

This study presents all the measured test results, such as: (1) crack load; (2) failure load; (3) the load-deflection at midpoint of the specimen; (4) crack patterns; and (5) failure modes. Tabs. 4 and 5 show the experimental results for all the tested specimens.

Specimen No.	P_i (kN)	P_f (kN)	Δ_i (mm)	Δ_f (mm)	S.S (mm)	D.D (-)	T (kN.mm)	Failure mode
RB1	568.11	731.39	11.53	16.64	54.60	2.13	3155.41	Diagonal shear failure mode
RB2	554.90	658.88	10.05	12.21	29.02	1.65	5031.36	
RB3	490.52	764.85	9.96	18.00	119.90	1.14	3846.74	
RB4	543.80	655.21	12.60	16.55	19.71	1.71	5456.65	
RB5	492.59	531.87	9.64	11.61	64.67	1.14	3818.48	
RB6	591.17	649.94	12.53	15.80	51.17	1.62	4225.15	
RB7	612.35	786.46	15.79	22.17	32.23	1.58	2731.72	
RB8	631.20	822.39	13.88	23.83	36.39	1.15	2359.86	
RB9	653.67	758.42	16.13	20.93	61.89	1.22	2130.18	

Table 4: Experimental results for all specimens.

Specimen No.	P_f/ $P_{f\ B1}$ %	$\Delta_f/\Delta_{f\ B1}$ %	S.S/S.S %	D.D/D.D %	T/T $_{RB1}$ %
RB1	100.00	100.00	100.00	100.00	100.00
RB2	97.67	73.38	53.15	77.46	159.45
RB3	86.34	108.17	219.60	53.52	121.91
RB4	95.72	99.44	36.10	80.28	172.93
RB5	86.71	69.77	118.44	53.38	121.01
RB6	104.06	94.95	93.72	76.06	133.90
RB7	107.79	133.23	59.03	74.18	86.57
RB8	111.11	143.21	66.65	53.99	74.79
RB9	115.06	125.78	113.35	57.28	67.51

Table 5: Experimental results compared to the control specimen (RB1).

First crack load and crack patterns

The load-deflection curves depicting the experimental outcomes for the nine specimens are illustrated in Fig. 8. It's evident that as the load increases, the deflection also rises until it reaches the failure load. Notably, a significant deflection transpired at the midpoint of each specimen. Once the failure load was attained, the load diminished while deflection continued to escalate. Parameters like secant stiffness, toughness, and displacement ductility were derived from these load-deflection curves and are presented in Tabs. 4 and 5.
The application of external reinforcement substantially enhances the specimens' capacity to withstand shear and torsion, leading to higher failure loads coupled with increased deflection, as evidenced in Fig. 8. Additionally, the specimens exhibited prolonged resistance before yielding to torsion failure. It's notable that the utilization of externally reinforced GFRP stirrups with a diameter of 12 mm (Specimen RB3) resulted in lesser deflection compared to the use of external GFRP stirrups with a diameter of 8 mm (Specimen B2), where deflection at failure load increased by 37%. Moreover, external GFRP stirrups at a 45º inclination (Specimen RB1), which offered superior strength, showed better performance than external stirrups at a 90º inclination (Specimen RB4). Fig. 9 presents the observed crack patterns in the retrofitted specimens subsequent to the addition of external GFRP stirrups.

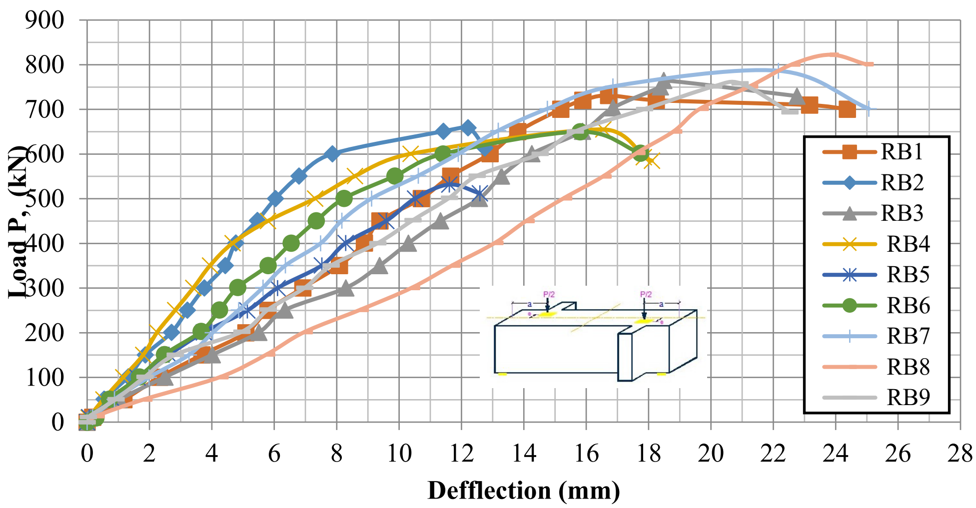

Figure 8: Experimental load-deflection curves for the strengthened specimens.

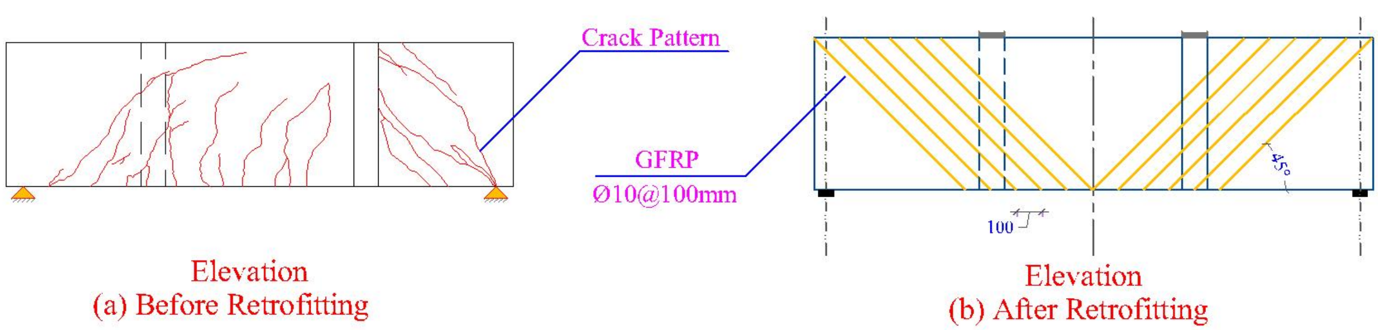

Figure 9: Crack pattern and retrofitting with external GFRP stirrups.

Failure modes

Specimens failed to shear, as shown in Fig. 10 and Tab. 4. At failure, there was a complete loss of stiffness observed by the sudden drop in load and the appearance of cracks in the compression face at the top of the specimen. The concrete cover of the bottom surface (the tension side) was separated. A few pieces of concrete fell, then the specimens failed in a diagonal shear mode outside the shear reinforcement zone.

Figure 10: Failure modes for the tested specimens.

LOAD DEFLECTION CURVES AND FAILURE LOADS

Load-deflection curves were graphed to investigate the impact of reinforcement on the global behavior of the reinforced box-section specimens. The outcomes have been detailed in Tab. 4. Across all examined specimens, three distinct phases of loading were evident. The initial stage displayed a rigid and linear response, wherein no substantial enhancement in stiffness was noted. This phenomenon could be attributed to the reinforcement's lack of contribution to resisting external loads until cracks are initiated. In the second stage, a non-linear response emerged, accompanied by a marginal decline in stiffness due to crack propagation and widening. Nonetheless, a slight upturn in stiffness was observable in this phase. The final loading stage demonstrated a marked reduction in specimen stiffness, coinciding with pronounced crack expansion and a moderate increase in their count.
Reinforced specimens displayed a notable augmentation in stiffness at this stage, in contrast to control specimens. Moreover, the formerly brittle shear failure of the control specimen transitioned into a partially ductile failure for the strengthened specimens, as detailed in Tab. 4. Fig. 11 visually portrays the crack and failure loads, crack-induced deflection, deflection at failure loads, and the load-deflection curves for all the experimental groups.

SECANT STIFFNESS (S.S.), DISPLACEMENT DUCTILITY (D.D.) AND TOUGHNESS (T)

Utilizing external strengthening exhibits an improvement in the secant stiffness (S.S.) of the specimens, as shown in Tabs. 4 and 5. The secant stiffness is enhanced for specimens RB2, and RB3 compared to the control specimen RB1 by 53.15% and 219.60%, respectively, which means that the diameter of the external stirrups has a significant effect on the behavior. The secant stiffness is enhanced for specimens RB4 and RB5 compared to the control specimen RB1 by 36.10% and 118.44%, respectively, which means that the GFRP stirrups inclination of the external strengthening has a significant effect on the secant stiffness and the pest inclination is 45 degrees. The secant stiffness is enhanced for specimens RB6, RB7, RB8, and RB9 compared to the control specimen RB1 by 93.72%, 59.03%, 66.65%, and 113.35%, respectively.

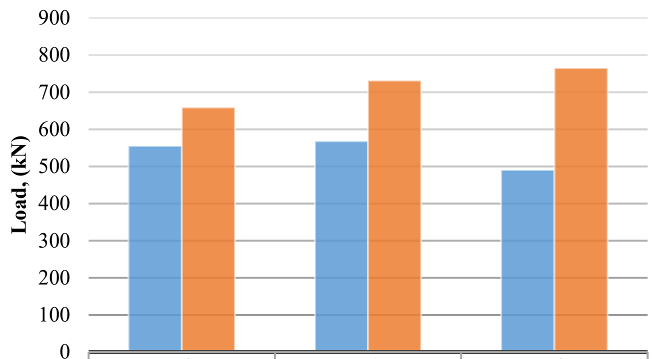

	B2	B1	B3
Pi	554,90	568,11	490,52
Pf	658,88	731,39	764,85

Group 1

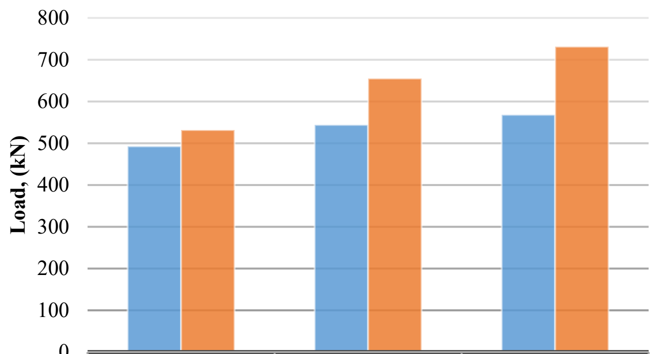

	B5	B4	B1
Pi	492,59	543,80	568,11
Pf	531,87	655,21	731,39

Group 2

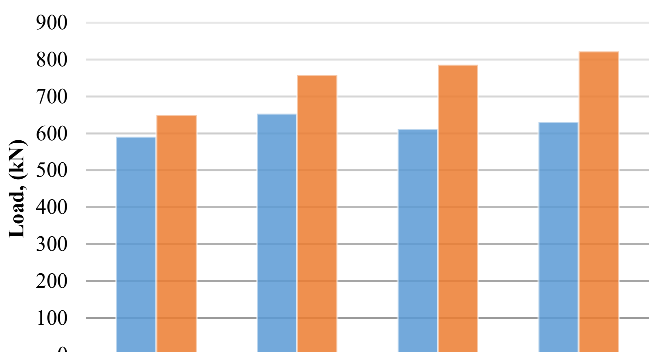

	B6	B9	B7	B8
Pi	591,17	653,67	612,35	631,20
Pf	649,94	758,42	786,46	822,39

Group 3

Figure 11a: Crack and failure loads.

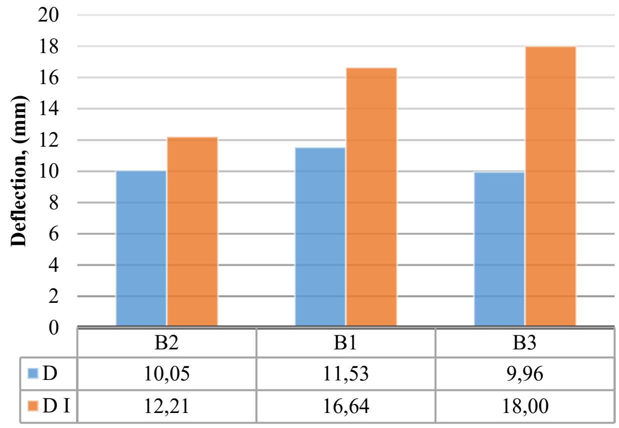

Group 1

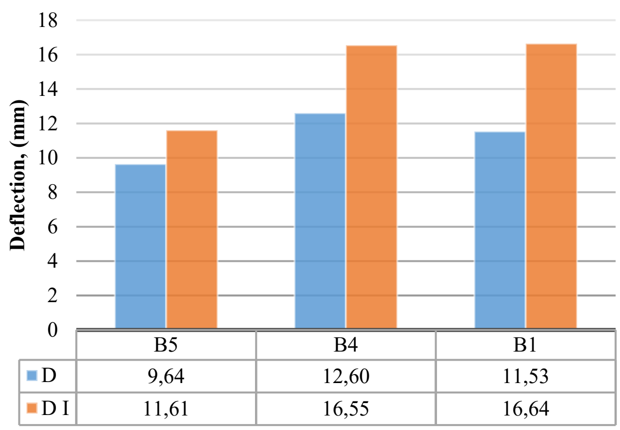

Group 2

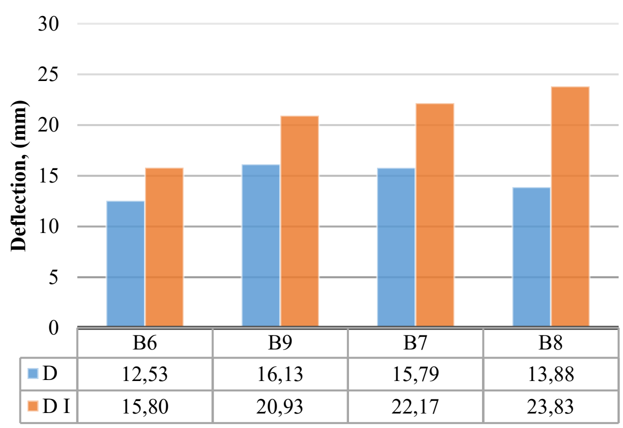

Group 3

Figure 11b: Deflection at the crack and failure loads.

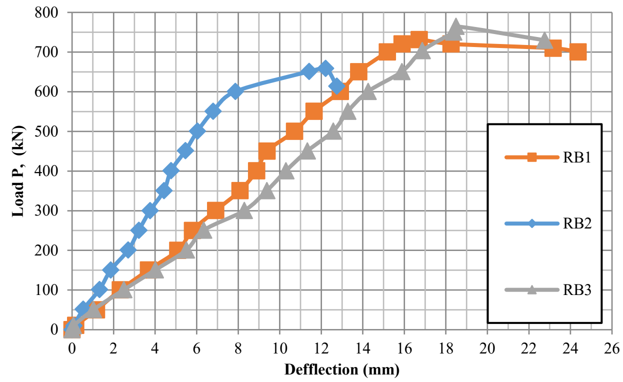

Group 1

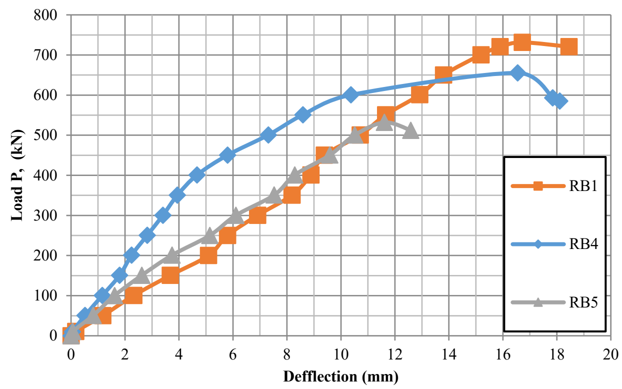

Group 2

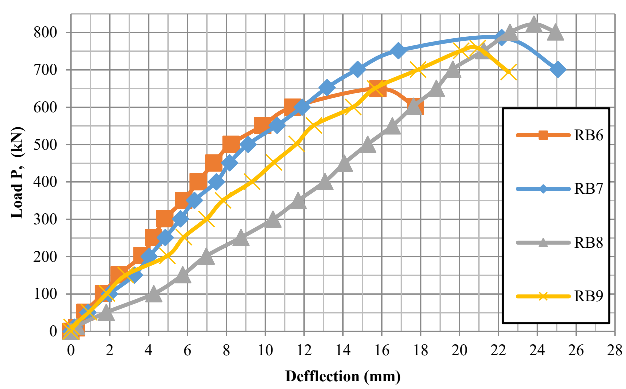

Group 3

Figure 11c: Effect of external GFRF stirrup spacing on the load-deflection curves.

Tab. 5 shows the test results compared to the control specimen, RB1. The displacement-ductility (D.D.) increased by 77.46%, 53.52%, 80.28%, 53.38%, 76.06%,74.18%, 53.99%, and 57.28 % for specimens RB2 to RB9 compared to the control specimen RB1.

Toughness (T) signifies the specimen's capacity to absorb deformations until reaching the failure load, quantified as the area beneath the load-deflection curve up to the point of failure (kN.mm). This parameter is a valuable metric for evaluating the specimen's ductility. In this investigation, the toughness exhibited improvement across all externally reinforced specimens. Specifically, toughness experienced enhancements in specimens RB2 to RB9, with increments of 159.45%, 121.91%, 172.93%, 121.01%, 133.90%, 86.57%, 74.79%, and 67.51%, respectively, when compared to the control specimen RB1. As a result, a marked enhancement in toughness was evident. Ultimately, the utilization of external strengthening via GFRP stirrups proves to be a highly effective approach for bolstering the toughness of the reinforced concrete specimens.

Effect of external GFRP stirrups diameter

By providing a larger reinforcement area, shear strength increased, as shown in Fig. 12, which illustrates the effect of changing the stirrups' diameters (Φ 8, Φ 10, and Φ 12 mm) on the failure load. An increase of 4.6% in the failure load has been recorded when Φ 12 stirrups (RB3) are used instead of Φ 10 stirrups (RB1). However, the failure load decreased by 11% with the use of 8-mm-diameter stirrups (RB2).

Effect of external GFRP stirrups inclination

The alignment of NSM stirrups significantly influences the enhancement of load capacity, particularly when positioned almost perpendicular to the diagonal crack trajectory (as seen in specimen RB1 with a 45-degree inclination). The specimens reinforced with inclined stirrups at 45 and 60 degrees (RB1 and RB4) displayed improvements of 27.3% and 10.4%, respectively, in contrast to the specimen employing vertical stirrups (RB5), as depicted in Fig. 13. As indicated in Tab. 4, the adoption of inclined strengthening stirrups instead of vertical ones led to a substantial improvement in failure load, resulting in a shift from brittle shear failure to a partially ductile mode of failure.

Effect of external GFRP stirrups spacing

Reducing the spacing between external stirrups emerged as a strategy that heightened the load-bearing capacity of the beams and facilitated a more even dispersion of reinforcing stirrups. This well-distributed arrangement led to the proliferation of numerous small-sized cracks. This mechanism effectively curtailed the expansion of major cracks as the applied load intensified, thereby enhancing both ductility and ultimate capacity. The correlation between failure load and stirrup spacing is graphed in Fig. 14. The chart indicates that reducing the gap between NSM GFRP stirrups is particularly advantageous when inclined stirrups are employed. However, their efficacy is less pronounced in the case of vertical stirrups. Furthermore, as delineated in Tab. 4, an increase in the spacing of NSM GFRP stirrups exerted a notable influence on the reduction of the initial crack load. This load decreased by 17% when spacing was set at 150 mm (RB6) and by 4% for spacing at 125 mm (RB9). Conversely, spacing at 75 mm (RB8) led to a 5% increase in crack load compared to the specimen with a spacing of 100 mm (RB7).

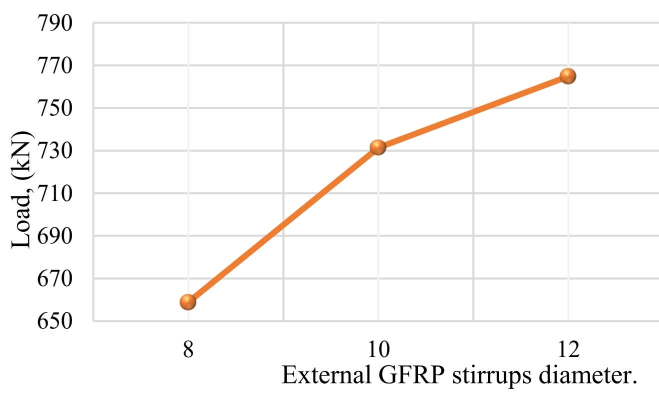

Figure 12: Effect of external GFRP stirrup diameter (Group 1).

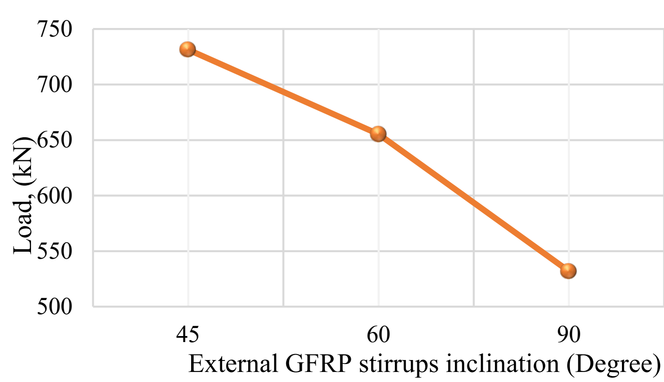

Figure 13: Effect of external GFRP stirrup inclination (Group 2).

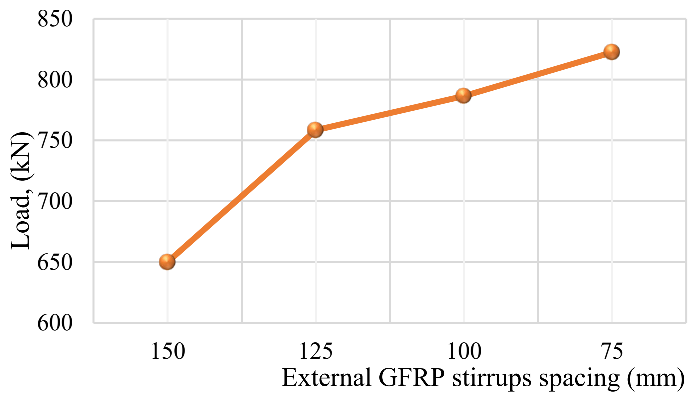

Figure 14: Effect of external GFRP stirrup spacing (Group 3).

Codes predictions

Many equations that have been suggested to evaluate the ultimate strength of reinforced concrete box sections. The equations of some codes, among them ECP-203 [24], ACI code [30], and CSA code [31], were concisely presented as per the following subsections:

Analysis according to ECP 203-2019 [24]

In step (1), determine cross-sectional parameters.
A_{oh} = area enclosed by the centerline of the closed stirrups;
P is the perimeter of the centerline of the closed stirrups.
In step (2), determine the GFRP torsion contribution (T_f) at the critical section using Eqn. (1):

$$A_{GFRP} = \frac{T_f * S * \sin\beta}{2A_\circ * \varepsilon_{fe} * E_{GFRP}} \tag{1}$$

where:
β: GFRP bar inclination;
A_{GFRP}: the area of GFRP ropes (stirrups);
A_0: the area enclosed inside the centerline of the shear flow = 0.85 A_{oh};
ε_{fe}: the effective strain level in FRP reinforcement;
E_{GFRP}: the tensile modulus of elasticity of GFRP; and
S: the spacing of stirrups.
In step (3), determine the ultimate torque moment (T_u). The ultimate torque moment is equal to the GFRP torsion contribution (T_f).

$$T_u = P_u * e \tag{2}$$

where e: the eccentricity of the load.

Analysis according to CI 318-19 [30]

The subsequent sequence of actions encapsulates the design guidelines presented in Chapter 11 of ACI 318-19 [30] for structural elements subjected to the combined influences of bending, shear, and torsion.
In step (1), determine the steel stirrups torsion contribution (T_s) at the critical section using the equation:

$$\frac{A_{str}}{S} = \frac{T_s}{2A_\circ * f_{yst} * \cot\theta} \tag{3}$$

where:
f_{yst}: is the yield strength of the steel stirrups;
A_{str}: is the area of one branch.
The torsion equations are based on the variable angle truss, where the angle θ (angle of inclination of the cracks) can be taken between 30 and 60 (recommended as 45 for reinforced concrete members).
In step (2), determine the GFRP torsion contribution (T_f) at the critical section using Eqn. (4):

$$\frac{A_{GFRP}}{S} = \frac{T_f * \sin\beta}{2A_\circ * \varepsilon_{fe} * E_{GFRP} * \cot\theta} \tag{4}$$

In step (3), determine the ultimate torque moment (T_u). The ultimate torque moment is equal to the sum of the steel torsion contribution (T_s) and the GFRP torsion contribution (T_f).

Analysis according to CSA A23.3-04 [31]

In step (1), determine the steel contribution to torsion (T_s), using Eqn. (5):

$$\frac{A_{str}}{S} = \frac{T_s}{2A_\circ * f_{yst} * \cot\theta} \tag{5}$$

The angle θ shall be taken as 35 according to the code requirements, where θ is the angle of inclination of the cracks.
In step (2), determine the GFRP torsional contribution (T_f) at the critical section using Eqn. (6):

$$\frac{A_{FRP}}{S} = \frac{T_f * \sin\beta}{2A_\circ * \varepsilon_{fe} * E_f * \cot\theta} \tag{6}$$

In step (3), determine the ultimate torque moment (T_u). The ultimate torque moment equals the sum of the steel torsion contribution (T_s) and the GFRP torsion contribution (T_f).

Specimen No.	$P_{f\ (Exp.)}$ (kN)	$P_{u\ (ECP[24])}$ (kN)	$P_{u(ECP[24])}/P_{f\ (Exp.)}$	$P_{u\ (ACI[25])}$ (kN)	$P_{u(ACI[30])}/P_{f\ (Exp.)}$	$P_{u\ (CSA[31])}$ (kN)	$P_{u(CSA[31])}/P_{f\ (Exp.)}$
RB1	731.39	609.07	0.83	609.07	0.83	869.84	1.19
RB2	658.88	389.80	0.59	389.80	0.59	556.70	0.84
RB3	764.85	877.05	1.15	877.05	1.15	1252.56	1.64
RB4	655.21	745.95	1.14	745.95	1.14	1065.33	1.63
RB5	531.87	380.01	0.71	380.01	0.71	542.71	1.02
RB6	649.94	406.04	0.62	406.04	0.62	579.89	0.89
RB7	786.46	609.07	0.77	609.07	0.77	869.84	1.11
RB8	822.39	812.09	0.99	812.09	0.99	1159.78	1.41
RB9	758.42	487.25	0.64	487.25	0.64	695.87	0.92
Average	-	-	0.83	-	0.83	-	1.18
Standard deviation	-	-	0.20	-	0.20	-	0.29

Table 6: Comparison of experimental and analytical results.

Analysis of the analytical results

Tab. 6 provides a concise overview of the analytical outcomes employing codes [24-31]. When examining the ultimate load and comparing analytical and experimental results, it becomes evident that the Egyptian and American codes tend to be more cautious in their estimations compared to the Canadian code. This conservative nature of the Egyptian and American codes, resulting in calculated results lower than the experimental ones, instills confidence in the applicability of the code's equations. In contrast, the Canadian code generates results that surpass those derived from experimentation. Averages and standard deviations for the code-based calculations are detailed in Tab. 6. Fig. 15 visually depicts the contrast between experimental and analytical results.

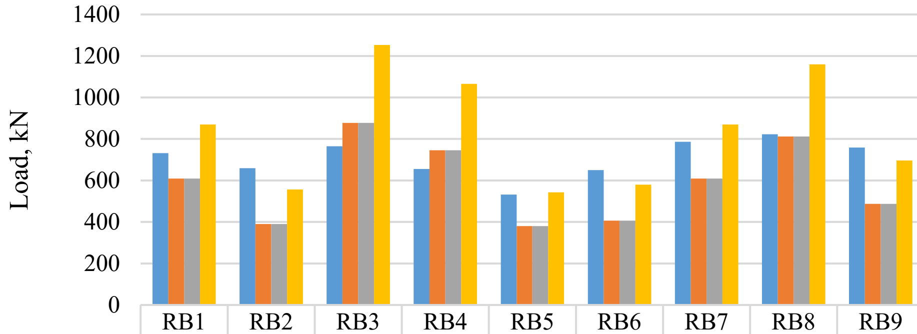

	RB1	RB2	RB3	RB4	RB5	RB6	RB7	RB8	RB9
Pu (Exp.)	731,39	658,88	764,85	655,21	531,87	649,94	786,46	822,39	758,42
Pu (ECP)	609,07	389,80	877,05	745,95	380,01	406,04	609,07	812,09	487,25
Pu (ACI)	609,07	389,80	877,05	745,95	380,01	406,04	609,07	812,09	487,25
Pu (CSA)	869,84	556,70	1252,56	1065,33	542,71	579,89	869,84	1159,78	695,87

Figure 15: Comparison of experimental and analytical results.

CONCLUSIONS

This paper focuses on using glass fiber-reinforced polymer GFRP ropes as near-surface mount stirrups. Nine box-section concrete specimens with dimensions of 2200 x 400 x 600 mm in length, width, and depth were decanted and tested. Based on the findings of the experimental program, the following points can be concluded:

1. The external GFRP stirrups' diameter, inclination, and spacing significantly affect the behavior of the strengthened specimens.
2. External strengthening improves the secant stiffness of the specimens, with a significant enhancement of 36.10% to 219.6%, according to the range of the studied parameters.
3. The diameter of the external stirrups significantly affects the secant stiffness.
4. Reducing the spacing between the NSM GFRP external stirrups improves the shear capacity by 4.6% to 11%, while the increase in stirrup spacing decreases the crack load.
5. Effective dispersion of external stirrups leads to the proliferation of numerous small-sized cracks. This mechanism effectively limits the enlargement of significant cracks as the applied load intensifies. As a result, decreasing the spacing of the stirrups enhances both ductility and ultimate load-bearing capacity.
6. The better distribution of the GFRP external stirrups improves ductility, leading to a significant increase in the initial crack load.
7. The toughness of the tested specimens was improved for all externally strengthened specimens, with significant enhancement ranging between 74.70% and 172.93% according to the range of the studied parameters. Consequently, significant improvement in toughness was observed. Therefore, using external strength with GFRP stirrups is an effective method to enhance the toughness of the reinforced concrete beams.
8. The external strengthening using GFRP stirrups transformed the brittle shear failure mode into a semi-ductile failure mode, where the displacement ductility increased by 53.38% to 80.28% according to the range of the studied parameters.
9. The orientation of NSM GFRP external stirrups has a significant effect on improving the shear capacity. The inclined stirrups show a considerable improvement of 27% compared to the vertical stirrups, leading to a transformation of the failure mode from brittle shear to semi-ductile failure. The pest inclination of stirrups is 45 degrees.
10. Changing the diameter of GFRP bars has a significant effect on shear strength, with a 5% increase in the load capacity observed when using 12 mm stirrups compared to 10 mm, while a decrease of 10% was observed when using 8 mm bars instead of 10 mm stirrups.
11. For the studied parameters, the provisions of the ACI, ECP, and CSA codes are conservative, which gives an underestimated ultimate torsion strength. Nonetheless, the CSA code considered the worth of extreme force higher than the overestimated exploratory outcomes.

ACKNOWLEDGMENTS

The authors acknowledge the technical support provided by the laboratory of the faculty of engineering at the American University of Cairo.

REFERENCES

[1] Hsu, T.C. (1984). Torsion of reinforced concrete. Van Nostrand Reinhold Company, New York, 516.
[2] Hearing, B.P. (2000). Delamination in reinforced concrete retrofitted with fiber-reinforced plastics. Ph.D. Thesis. Massachusetts Institute of Technology. Cambridge, Massachusetts, United States.
[3] Chidananda, S.H., and Khadiranaikar, R.B. (2017). Flexural behavior of concrete beams reinforced with GFRP rebars. International Journal of Advanced Research. Ideas, and Innovations in Technology.
[4] Rahal, K.N., and Rumaih, H.A. (2011). Tests on reinforced concrete beams strengthened in shear using near-surface-mounted CFRP and steel bars. Engineering Structures, 33(1), pp. 53–62. DOI: 10.1016/j.engstruct.2010.09.017
[5] Shanour. A.S., Mahmoud. A.A, Adam, A.M., and Said, M. (2014). Experimental investigation of concrete beams reinforced with GFRP bars. International Journal of Civil Engineering and Technology (IJCIET), 5(11), pp. 154-164.
[6] Adam, A.M., Said, M., Mahmoud, A.A., and Shanour, A.S. (2015). Analytical and experimental flexural behavior of concrete beams reinforced with glass fiber-reinforced polymer bars. Construction and Building Materials (84), pp. 354–366. DOI: 10.1016/j.conbuildmat.2015.03.057
[7] Täljsten, B., Carolin, A., and Nordin, H. (2003). Concrete structures strengthened with near-surface-mounted reinforcement of CFRP. Advanced Structure Engineering, 6 (3), pp. 201–213. DOI: 10.1260/136943303322419223
[8] Warren, G.E. (1998). Waterfront repair and upgrade, Advanced Technology Demonstration Site No. 2: Pier 12, NAVSTA San Diego, Site Specific Report SSR-2419-SHR, Naval Facilities Engineering Service Center, Port Hueneme, CA.
[9] El-Hacha, R., and Rizkalla, S.H. (2004). Near-surface-mounted fiber-reinforced polymer reinforcements for flexural strengthening of concrete structures, Structural Journal, 101(5), pp. 717–726. DOI: 10.14359/13394.
[10] Harba, I., Abdulridha, A., and Al Shaar, A. (2023). Numerical analysis of reinforced concrete circular columns strengthened with CFRP under concentric and eccentric loadings, Frattura ed Integrità Strutturale, (63), pp. 190-205. DOI: 10.3221/IGF-ESIS.63.16
[11] Cunha, R., Oliveira, K., Brito, A., Vieira, C., and Amorim, D. (2021). Evaluation of the behavior of reinforced concrete beams repaired with glass fiber-reinforced polymer (GFRP) using a damage variable, Frattura ed Integrità Strutturale, 15(57), pp. 82–92. DOI: 10.3221/IGF-ESIS.57.08.
[12] Raj, S.D., and Suruti, R.S. (2012). Shear strengthening of reinforced concrete beams using near surface mounted glass fiber reinforced polymer, Asian Journal of Civil Engineering, (13), pp. 679–690.
[13] Samad, A. A., Hassen, D.R., Mohamad, N., Attiyah, A.N., Jayaprakash J., Mendis, P., Zainorizuan, M.J., Yee Yong L., Alvin, L., Siang, J.M., Hanifi, O.M., Nazahiyah, R.S., and Shalahuddin, A.M. (2017). Shear rehabilitation of RC deep beams using NSM CFRP anchor bars, MATEC Web Conference, 103-02010, DOI: 10.1051/matecconf/201710302010.
[14] Al-Mahmoud, F., Castel, A., François, R., and Tourneur, C. (2009). Strengthening of RC members with near-surface mounted CFRP rods, Composite Structure, 91(2), pp. 138–147.
[15] De Lorenzis, L., Nanni, L., and Tegola, A.L. (2000). Strengthening of reinforced concrete structures with near-surface-mounted FRP rods, International Meeting on Composite Materials, PLAST 2000, Proceedings, Advancing with Composites, , pp. 9–11.
[16] Lorenzis, L. D., and Nanni, A. (2001). Shear strengthening of reinforced concrete beams with near-surface mounted fiber-reinforced polymer rods, ACI Structural Journal, 98(1), pp. 60–68.
[17] Mezher, T.M. (2015). Shear strengthening of RC deep beams with near—surface-mounted CFRP rods, Ph.D. Thesis, University of Basrah.
[18] Kishi, N., Mikami, H., Kurihashi, Y., and Sawada, S. (2005). Flexural behavior of RC beams reinforced with NSM AFRP rods, Proceedings of the International Symposium on Bond Behavior of FRP in Structures (BBFS 2005), International Institute for FRP in Construction, pp. 337–342.
[19] De Lorenzis, L., and Teng, J.G. (2007) Near-surface-mounted FRP reinforcement: An emerging technique for strengthening structures. Composite Part B: Engineering, 38(2), pp. 119-143. DOI: 10.1016/j.compositesb.2006.08.003.

[20] Parretti, R., and Nanni, A. (2004) Strengthening of RC members using near-surface-mounted FRP composites: Design overview. Advanced in Structural Engineering, 7(6), pp. 469-483.
[21] Täljsten, B., Carolin, A., and Nordin, H. (2001). Concrete beams strengthened with near-surface-mounted CFRP laminates. In Proceedings of CFRPCS-5, C. Burgoyne (ed.). Cambridge, UK, pp. 107-116.
[22] Täljsten, B., Carolin, A. and Nordin, H. (2003). Concrete structures strengthened with near-surface-mounted reinforcement of CFRP. Advanced in Structural Engineering, 6(3), pp. 201-221. DOI: 10.1260/136943303322419223
[23] El-Hacha,R., and Rizkalla, S.H. (2004). Near-surface-mounted fiber-reinforced polymer reinforcements for flexural strengthening of concrete structures. ACI Structural Journal, 101(5), pp. 830-839. DOI: 10.14359/13394
[24] Egyptian Code of Practice for Design and Construction of Reinforced Concrete Structures, ECP-203. (2019). Housing, and Building Research Center, Ministry of Building and Construction, Giza, Egypt, Chapter 6,113-122.
[25] ASTM D790-02. (1998). Standard Test Methods for Flexural Properties of Unreinforced and Reinforced Plastics and Electrical Insulating Materials, American Society of Mechanical Engineering, New York. DOI: 10.1520/D0790-02
[26] ASTM International (2021): Standard test method for static modulus of elasticity and Poisson ratio of concrete in compression, ASTM C469/C469M-14, West Conshohocken. DOI: 10.1520/C0469_C0469M-14.
[27] ASTM International (2015): Standard test method for splitting tensile strength of cylinder concrete specimens, ASTM C496-96. DOI: 10.1520/C0496-96
[28] ASTM International (2015): Standard test method for compressive strength of cylindrical concrete specimens, ASTM C39/ C39M–14. DOI: 10.1520/C0039 C0039 M-14
[29] ASTM D7205 Tensile Tests of GFRP Matrix Composite Bars
[30] ACI Committee 318-19. (2019). Building Code Required for Reinforced Concrete, (ACI 318-19) and Commentary (ACI 318R-19), American Concrete Institute, Farmington Hills, Mich. DOI: 10.14359/51716937
[31] CSA-A23.3-04, (2004), Design of Concrete Structures for Buildings, Canadian Standards Association, Rexdale, Ontario, Canada. 240 p.

NOMENCLATURE

a : Shear span - the distance from the load to the support (400, 450, and 600 mm);
b : Specimen width (constant at 400 mm);
d : Specimen effective depth (= total depth –concrete cover (25 mm) =575 mm (constant));
t : Specimen depth = 600 mm (constant);
L_0 : Specimen's clear span (constant at 2000 mm);
a/t : Shear-span to total depth ratio (0.67, 0.75, and 1.0);
e : Eccentricity of the applied load from the center of the specimen axis;
A_s : Area of GFRP bars in tension (constant at 8Φ12);
$A_s`$: Area of GFRP bars in compression (constant at 4Φ8);
f_{cu} : Cubic concrete characteristic compressive strength of 25 MPa;
$f_c`$: Cylindrical concrete characteristic compressive strength (20 MPa);
GFRP: Glass Fiber Reinforced Plastic;
P_i : First crack load before retrofitting;
P_{fR} : Failure load after retrofitting;
Δf_i : Displacement at mid-span at failure load before retrofitting;
Δ_{fR} : Displacement at mid-span at failure load after retrofitting;
S.S : Secant stiffness (N/mm) P_{fR}/Δ_{fR};
D.D : Displacement ductility is the ratio of the deflection at 90% of the failure load in the descending branch to that in the ascending branch; and
T : Toughness is the ability to adsorb deformations up to failure, which equals the area under the load-deflection curve up to failure.